Photoelectric emission from negative-electron-affinity diamond (111) surfaces: Exciton breakup versus conduction-band emission

C. Bandis and B. B. Pate
Department of Physics, Washington State University, Pullman, Washington 99164-2814
(Received 3 April 1995; revised manuscript received 11 July 1995)

We have recently reported that bound electron-hole pairs (Mott-Wannier excitons) are the dominant source of photoelectron emission from specially prepared ["as-polished" C(111)-(1×1):H] negative-electron-affinity diamond surfaces for near-band-gap excitation up to 0.5 eV above threshold [C. Bandis and B. B. Pate, Phys. Rev. Lett. **74**, 777 (1995)]. It was found that photoexcited excitons transport to the surface, break up, and emit their electron. In this paper, we extend the study of exciton-derived emission to include partial yield (constant final-state) analysis as well as angular distribution measurements of the photoelectric emission. In addition, we find that exciton-derived emission does not always dominate. Photoelectric emission properties of the *in situ* "rehydrogenated" (111)-(1×1):H diamond surface are characteristically different than emission observed from the as-polished (111)-(1×1):H surface. The rehydrogenated surface has additional downward band bending as compared to the as-polished surface. In confirmation of the assignment of photoelectric yield to exciton breakup emission, we find a significant enhancement of the total electron yield when the downward band bending of the hydrogenated surface is increased. The functional form of the observed total electron yield demonstrates that, in contrast to the as-polished surface, conduction-band electrons are a significant component of the observed photoelectric yield from the *in situ* hydrogenated (111)-(1×1):H surface. Furthermore, electron emission characteristics of the rehydrogenated surface confirms our assignment of a Fan phonon-cascade mechanism for thermalization of excitons.

I. INTRODUCTION

The inability of a classical approach to properly describe photoelectric emission phenomena was seminal in the development of quantum theory. The physics of the photoelectric effect was resolved by Einstein[1] in 1905 with the introduction of the quantum nature of light. Photoelectric emission is today a well-understood process, which has evolved into a powerful technique for the study of the electronic[2] and geometric[3] structure of solids and surfaces. Here, we apply Spicer's three-step model[4,5] for photoelectric emission to the study of bulk-to-surface transport and electron escape phenomena from prepared diamond (111) surfaces. The fundamental characteristics of electron transport and escape determined by photoelectric measurement have a direct bearing on transport and escape properties of electrons injected into the diamond conduction band by other (e.g., electronic) means.

In contrast to common understanding, we have recently reported[6] that bound electron-hole pairs (Mott-Wannier excitons) are the source for photoelectron emission from specially prepared [as-polished diamond C(111)-(1×1):H] negative-electron-affinity diamond surfaces when excited with near-band-gap radiation. In this special case, photoelectric emission is dominated by photoexcited excitons, which transport to the surface, whereupon the exciton is broken apart and the electron is emitted. However, exciton-derived emission does not always dominate. Photoelectric emission properties of the *in situ* rehydrogenated (111)-(1×1):H diamond surface are characteristically different than emission observed from the as-polished surface. The rehydrogenated surface has additional downward band bending, as compared to the as-polished surface. In confirmation of the exciton breakup emission mechanism, we find a significant enhancement of the total electron yield, when the downward band bending of the hydrogenated surface is increased. The functional form of the observed total electron yield demonstrates that, in contrast to the as-polished surface, conduction-band electrons are a significant component of the observed photoelectric yield from the *in situ* rehydrogenated (111)-(1×1):H surface. Furthermore, the absence of spectral oscillations in the photoelectric yield of the rehydrogenated surface confirms our assignment of a Fan phonon-cascade mechanism for the thermalization of hot excitons in diamond.

II. BACKGROUND

A. Negative electron affinity

A typical band scheme of a semiconductor surface is shown in Fig. 1(a). The vacuum lies above the conduction-band minimum (CBM) creating an energy barrier, the electron affinity (χ), which prevents low-energy electrons from escaping into the vacuum. If the vacuum level lies below the CBM energy at the surface, then $\chi<0$ and a *true* negative-electron-affinity (NEA) surface is produced [Fig. 1(c)]. The occurrence of *true* NEA has not been found for conventional semiconductor materials (e.g., Si, Ge, GaAs, InP, etc.) and is thought by many to never occur. Conventional NEA semiconductor surfaces are, however, prepared by the engineered com-

0163-1829/95/52(16)/12056(16)/$06.00

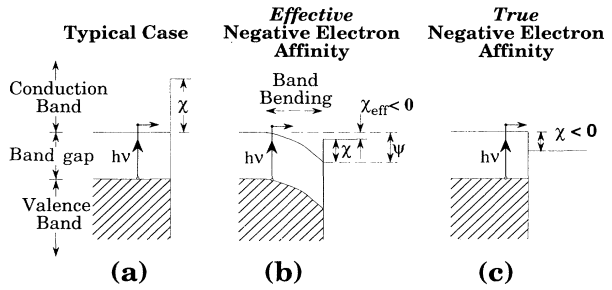

FIG. 1. Electron affinity band diagrams showing (a) positive electron affinity, (b) effective negative electron affinity, and (c) true negative electron affinity.

bination of heavy p-type doping together with cesium or cesium oxide surface coatings.[7] Cesium oxide (or cesium) is deposited as ionic species in monolayer quantities to form an affinity lowering surface dipole. This reduction in the electron affinity, together with a short characteristic band bending length (due to heavy p-doping) results in an *effective* negative-electron-affinity surface [Fig. 1(b)]. In contrast, self-consistent local-density-based methods[8] have found that cesium on oxygenated diamond (100) should produce a *true* NEA surface. Furthermore, *ab initio* local-density-based calculations[9] have found that the diamond (100)-(2×1):H is *true* NEA. A NEA semiconductor surface (whether *true* NEA or *effective* NEA) makes it possible for bulk conduction-band electrons with kinetic energies as low as the CBM to escape into the vacuum. Over the years, NEA semiconductor surfaces have been used to create efficient electron emitters utilized in devices such as photocathodes, electron multipliers, and other tools essential to both science and technology.

An experimental determination of the presence of NEA is to photoexcite valence-band electrons to the CBM and observe the electron emission that occurs. Emission at excitation photon energies as low as the band-gap energy will only occur if the electron affinity is negative (either *true* or *effective).* The presence of NEA can also be confirmed by observing whether the low-kinetic-energy threshold of the electron energy distribution curves (EDC) coincide with the CBM. In this case, the emission width (W) of the EDC's (from the low-kinetic-energy threshold to the valence-band-maximum emission) is given by $W=h\nu-E_g-\chi$, so that $\chi=h\nu-E_g-W$. A NEA surface makes it possible for secondary electrons, which thermalize down to the CBM to be emitted into the vacuum. Many factors, including the multiplication of carriers due to electron-electron scattering, and the much greater diffusion length of thermalized carriers at the CBM as compared to the inelastic mean free path[10] at higher kinetic energies contribute to a narrow and intense emission for CBM electron emission from NEA material. Therefore, a qualitative test for NEA is to observe an intense emission at low kinetic energy, indicative of thermalized carrier emission.

Himpsel *et al.*[11] first demonstrated that the (111)-(1×1):H diamond surface has negative electron affinity. They based their NEA assignment upon the appearance of a photoelectric threshold at the band-gap energy of 5.5 eV, by analysis of the width of the electron kinetic-energy distribution, and by the observation of a sharp peak in the kinetic-energy distribution indicative of thermalized carrier emission. In contrast, the (111)-(2×1) reconstructed diamond surface has been determined[12,13] to have positive electron affinity. NEA activation of the (111) diamond surface by hydrogen adsorption has been achieved by a variety of means including (a) mechanical polishing in olive oil followed by solvent degreasing,[13] (b) exposure of the clean surface at room temperature to atomic hydrogen,[13] (c) cleavage in molecular hydrogen at atmospheric pressure,[14] and (d) exposure of the surface to hydrogen plasmas.[15] Other preparations[16,17] have produced diamond surfaces that exhibit NEA characteristics. Van der Weide and Nemanich[16] demonstrated that NEA results from the deposition of a thin titanium layer on a hydrogen free, positive-electron-affinity (111) diamond surface. In addition, it has been found that diamond negative-electron-affinity effects are not limited to the (111) surface. Both the monohydride (100)-(2×1) (Refs. 18–20) and the adsorbate-free (100)-(2×1) diamond surface with monolayer coverage of Ni (Ref. 21) have been reported to exhibit NEA.

B. Photoexcitation of bound and unbound electron-hole pairs

The band gap of diamond [$E_g=5.49\pm0.005$ eV at $T=100$ K (Ref. 22)] is indirect. Similar to silicon, the CBM lies in the [100] direction, and is located at a wave vector $k_{\mathrm{CBM}}=(0.76\pm0.02)k_x$ between the zone center (Γ_1) and the zone boundary (X_1).[22] At excitation photon energies near band to band absorption thresholds, experimental measurements of the adsorption coefficient can be understood only if one includes the interaction between the electrons and holes produced during photoabsorption.[23–25] The mutual Coulomb attraction between electrons and holes allows bound states, *excitons,* to be formed in the crystal with energy less than that of the free pair of particles.[26] The exciton reduced mass and dielectric constant distinguishes between *Mott-Wannier excitons,* which have radius of at least a few lattice constants and are free to move through the crystal, and *Frenkel excitons,* which have a radius comparable to the interatomic distance and become localized, resembling an atomic excited state.[26,27] Intrinsic excitons in diamond have a radius of about 15 Å,[28] which is ten times larger than the nearest-neighbor distance (1.54 Å), and, therefore, are considered to be Mott-Wannier excitons. The Mott-Wannier exciton binding energy in diamond is $E_x=80\pm5$ meV.[22,29]

Photoexcitation of an electron from the valence-band maximum (VBM) to the CMB in diamond (creation of an *unbound* electron-hole pair) proceeds via an indirect transition, which involves the simultaneous absorption of a photon ($h\nu$) with either phonon ($\hbar\omega$) emission ($h\nu-\hbar\omega=E_g$) or phonon absorption ($h\nu+\hbar\omega=E_g$). Threshold photoexcitation into *bound* electron-hole pairs

(excitons) similarly proceeds via an indirect transition ($h\nu \pm \hbar\omega = E_{gx}$), where E_{gx} denotes the indirect exciton energy gap. By lowering the temperature of the sample under study, the population of phonons is diminished so that the first process, photon absorption with phonon emission, becomes dominant. Photoabsorption measurements from diamond have demonstrated[29] that cooling below 180 K is sufficient to ensure that photon absorption with simultaneous phonon generation dominates. Therefore, by performing experiments at low temperatures, we lower the number of thresholds in the absorption and simplify the analysis of the observed spectra.

When a bound pair is formed, the electron and hole must be at the same position in the crystal and so are preferentially excited into states in which they are most likely to be together. In the case of an indirect transition and assuming isotropic bands, Elliot[25] showed that the absorption coefficient component for each phonon contribution will rise as the square root of the excess energy,

$$\alpha_{\rm ex} \propto (h\nu - E_{gx} \pm E_{\rm ph})^{1/2} , \quad (1)$$

for allowed indirect transitions into *bound* electron-hole pairs (i.e., excitons), and as the $\frac{3}{2}$ power for excitation into *unbound* electron-hole pairs (creation of free conduction-band electrons),

$$\alpha_{\rm el} \propto (h\nu - E_g \pm E_{\rm ph})^{3/2} , \quad (2)$$

where E_{gx} is the exciton gap, and E_g is the band gap.

Consistent with theory, Dean and co-workers[22,29] identified the dominant indirect transitions ($h\nu \geq 5.54$ eV) that account for intrinsic photoabsorption in diamond. The two strongest components ($h\nu \geq 5.54$ eV) of the photoabsorption coefficient at $T = 100$ K (Ref. 29) are

$$\alpha = A(h\nu - 5.54)^{1/2} + B(h\nu - 5.615)^{3/2} , \quad (3)$$

with $A = 2855$ cm^{-1} eV$^{-1/2}$ and $B = 21\,508$ cm^{-1} eV$^{-3/2}$. Consistent with theory,[24,25] Clark, Dean, and Harris[29] identified the first component ($\frac{1}{2}$ power law) with exciton producing indirect transitions, and the second ($\frac{3}{2}$ power law) with indirect transitions, which create unbound electron-hole pairs (i.e., "free electrons" and "free holes").

C. Exciton effective mass

In contrast to the ideal case of a semiconductor with simple parabolic bands, an exact analytical solution of the exciton energy dispersion curves is not possible[30] for semiconductors with both degenerate valence-band maxima and anisotropic conduction-band minimum. However, a satisfactory theoretical approach for indirect excitons that takes into full account both the degeneracy and the anisotropy of the bands, and allows for accurate numerical solution of the problem has been developed by Altarelli and Lipari.[31,32] Their results find[31] that the longitudinal and transverse excitons of both Si and Ge exhibit a remarkable hydrogenlike parabolicity ($E = \hbar^2 k^2 / 2M$), which can be described approximately by the sum, M, of the electron mass to the average hole mass. In addition they introduce the parameter λ, which for anisotropic bands is a function of direction and is defined in terms of the electron, and both light- and heavy-hole masses ($m_{\rm lh}, m_{\rm hh}$), and is the difference in the center-of-mass position of an electron-hole pair when the hole is heavy or light, divided by the pair separation:

$$\lambda = \frac{2m_e \Delta m_h}{(m_e + m_h)^2 - \Delta m_h^2} \quad (4)$$

where m_e is the transverse or longitudinal electron effective mass, $m_h = m_{\rm lh} + m_{\rm hh}/2$, and $\Delta m_h = m_{\rm lh} - m_{\rm hh}/2$. This quantity, which varies between 0 and 1, is an estimate of how well the center of mass is defined. Therefore, one expects parabolic dispersion for small λ, and deviations from parabolicity, as well as dependence of the exciton mass on the exciton state when λ is a significant fraction of 1. For the longitudinal exciton in silicon (germanium) with $\lambda = 0.18$ ($\lambda = 0.14$) the parabolicity is indeed remarkable, and the difference of the approximate exciton mass (M) to the numerically calculated mass is about 7% or less.[31] Following the same approach in diamond, and using the hole effective masses reported by Kono *et al.*[33] ($m_{\rm lh} = 0.3m_0$, and $m_{\rm hh} = 0.75m_0$), and the electron effective masses reported by Nava *et al.*[34] ($m_l = 1.4m_0$, and $m_t = 0.36m_0$, where m_0 is the free-electron mass), we find $\lambda_{\rm long} = 0.17$, $\lambda_{\rm trans} = 0.22$, and $M_{\rm long} = 1.9m_0$, $M_{\rm trans} = 0.9m_0$. Since the value of λ for diamond is comparable to the values obtained for silicon and germanium, we expect that exciton dynamics in diamond are accurately described by a parabolic dispersion characterized by the hydrogenlike effective masses $M_{\rm long}$ and $M_{\rm trans}$.

D. The three-step model of photoelectric emission

Photoelectric emission is a bulk effect and can be understood in terms of a three-step model (as developed by Spicer[4]) consisting of (a) bulk *excitation,* absorption of light generates photoexcited carriers; (b) *transport* of the carriers to the surface region; and (c) *escape* of the electrons from the surface into the vacuum (see Fig. 2).

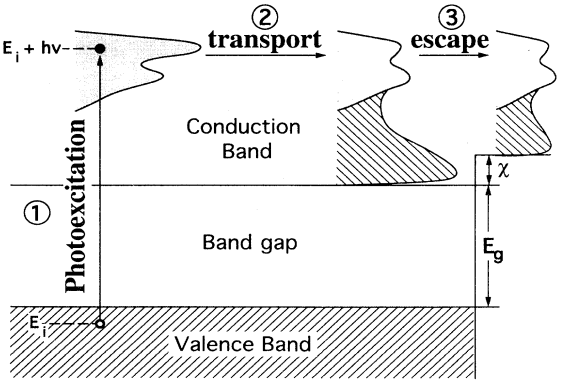

FIG. 2. The three-step model of photoemission. (1) photoexcitation, (2) transport, (3) escape (after Ref. 35).

Spicer assumed that photogenerated bulk carriers transport to the surface via a random walk or diffusion model. Carriers which arrive at the surface escape according to a probability factor, $P(h\nu)$. It is clear that the three-step model applies equally well to other photogenerated mobile carriers (such as *Mott-Wannier excitons)* that could lead to electron emission and which are consistent with the simple assumptions concerning transport and escape. The general case for near-band-gap photoelectric emission from diamond is when electron emission occurs as the result of both electron and exciton transport to the surface. In such a case, we allow for two independent transport and escape steps to describe the behavior of excitons and electrons, respectively. The total electron yield is given by the sum of the two components:[5,7]

$$Y(h\nu)=\sum Y_i \ ,$$

where

$$Y_i=P_i(h\nu)\frac{L_i(h\nu)\alpha_i(h\nu)}{1+L_i(h\nu)\alpha(h\nu)} \ , \tag{5}$$

where i=excitons or electrons, $\alpha_{ex}(h\nu)=A(h\nu-5.54)^{0.5}$, $\alpha_{el}(h\nu)=B(h\nu-5.615)^{1.5}$, and $\alpha(h\nu)=\alpha_{ex}(h\nu)+\alpha_{el}(h\nu)$ as presented in Eq. (3). L_i are the carrier diffusion lengths, which at a given temperature should be a property of the bulk crystal, and P_i are surface escape probabilities, which should be a function of the surface treatment and condition.

If it is assumed that the majority of the carriers rapidly thermalize[35] to the bottom of the band, and if thermalized carriers can result in electron escape, then the diffusion length of the thermalized carrier $L(h\nu)$ should be independent of the initial energy of the carrier, and so independent of the excitation photon energy. Even in the case of a NEA semiconductor surface, not every electron that reaches the surface will be emitted due to quantum-mechanical reflection at the vacuum-solid interface and another related effects. However, the probability for escape, $P(h\nu)$ should be independent of the excitation energy if the carriers are thermalized before reaching the surface. In practice,[5,7] the three-step model has successfully modeled the total electron yield for effective NEA photocathodes by using an energy-independent characteristic transport length L and an energy-independent probability factor P.

III. EXPERIMENTAL METHODS

A. Sample description and preparation

This work was performed on the (111) surface of a four carat, type-IIb natural single-crystal diamond (our sample D5).[36] Type IIb denotes p-doped (boron) semiconducting diamond. The (111) surface studied was 7×5 mm,^{2} and the color of the crystal was light brown with a tone of pale blue. Before each study, the diamond surface was mechanically polished on a 10 in. cast iron wheel, using 1-μm grit and olive oil, under a load of several pounds. Several micrometers of diamond were typically removed and a fresh (111)-(1×1):H surface was prepared with each polishing. The cast iron wheel was typically run at 600 rpm, and the diamond radially traversed the wheel during polishing in a cyclic manner. During polishing, the grit itself erodes and the olive oil may act as a source of hydrogen. This general polishing technique, which has been used by the jewelers for well over a century,[37] is the same that we employed in earlier studies,[13] and is recently reviewed by Wilks and Wilks.[38] During polishing, the sample was bonded to the goniometer by the use of an epoxy (Buehler Epoxide), which was removed after the polishing had been completed by heating the fixture (with sample attached) in air to 200°C. The single crystal was then cleaned by ultrasonic rinse in methyl-ethyl-ketone, acetone and alcohol, followed by a light hand polish with lens paper and/or cotton tipped applicators.

B. The ultrahigh-vacuum apparatus

The photoemission experiments were performed in an all-metal ion-pumped ultrahigh-vacuum (UHV) chamber. The base pressure after a 12-h bake at 150°C was $\leq 5\times10^{-11}$ Torr. The samples were mounted, using platinum foil and wire, onto a liquid nitrogen cooled sample holder, and positioned at the center of the chamber. A tungsten filament mounted behind the sample was used for electron-beam heating. Sample temperatures from 130 K up to 1400 K were routinely achieved. Temperature measurements were performed using a chromel-alumel thermocouple, spot welded to the platinum support in contact with the back side of diamond samples. *In situ* rehydrogenation of the diamond surface was achieved by room-temperature exposure of the diamond to a flux of atomic hydrogen. Atomic hydrogen was produced by a hot tungsten filament operated at a nominal temperature of 1900°C, which was monitored with an optical pyrometer. The hot filament was situated about 3 in. away from the sample surface. A 5–10 min exposure at 2×10^{-5} Torr (molecular hydrogen background) was typical in order to achieve saturation coverage.

C. Electron spectroscopy and photoelectric yield techniques

Two different electron detectors were used to perform photoemission and photoyield experiments. An electrostatic hemispherical mirror analyzer (VG Clam 100) was used to measure the emitted electron energy distributions. The electron energy analyzer was operated with an energy resolution of 80 meV, when ultraviolet photoemission spectroscopy (UPS) measurements were performed, and 0.8 eV during x-ray photoelectron spectroscopy (XPS) experiments. A single-electron counting, position sensitive, multichannel plate detector (Quantar) was used[39] to measure the total electron yield and the electron angular distributions. Samples were biased (-5–-20 V) during the UPS and photoelectric yield measurements to raise the kinetic energy of the emitted electrons above the work function of the electron detector. Other than overcoming the work function of the energy analyzer, no significant changes in the electron energy distributions were observed as a function of bias.

A dual anode Al $K\alpha$/Mg $K\alpha$ Perkin-Elmer x-ray source was used for the XPS measurements. During the experiments, the front window of the x-ray source was abut 0.5 in. away from the sample surface under study. The angle between the x-ray source and the analyzer was 83°, and the sample normal was facing about 40° away of the analyzer. A home built, differentially pumped, noble gas resonance lamp[40] similar to the one built by Yu,[41] was employed for the UPS measurements using He I (21.2 eV) and He II (40.8 eV) lines. Radiation from the resonance lamp passed through a simple grating monochromator[42,43] and refocusing system[40] before resulting in a 2-mm diameter spot on the sample surface. A 1-m vacuum UV scanning monochromator (McPherson, model 225) with a 1000 W, Hg-Xe discharge lamp was used as the source of continuous monochromatic radiation in the energy range of 5–6.5 eV. The Hg-Xe lamp was operated at a current of 20 A, instead of the suggested 28.5 A, in order to enhance UV output intensity. The refocusing system consisting of a 2-m radius of curvature platinum coated concave mirror and a Al-MgF_2 coated flat mirror, was arranged to produce 1:1 image of the exit slit of the monochromator on the sample position. The energy resolution of the light was always less than 50 meV. The excitation spectra were normalized with respect to the photoyield of sodium salicylate ($NaC_7H_5O_3$).[44] Watanabe and Inn[95] have characterized the photoyield of sodium salicylate over the wavelength range from 800 Å up to 2800 Å. Its flat response together with its long term stability, make sodium salicylate ideal for photon flux normalization versus photon energy. Absolute calibration of the sodium salicylate photoyield was accomplished by comparison to the quantum yield of gold, as reported by Krolikowski and Spicer.[46]

IV. RESULTS AND DISCUSSION

A. Surface characterization

1. *Properties of the diamond (111) surface*

The "as-polished" (111) diamond surface is known to be hydrogen terminated.[12,13,47–49] Immediately upon insertion into vacuum, the as-polished (111) surface exhibits a 1×1 low-energy-electron-diffraction (LEED) pattern. Upon annealing above 1000°C, the LEED changes to a reconstructed 2×2/2×1 pattern. This reconstructed diamond surface is hydrogen free.[13,49] The 2×1 π-bonded chain structure of Pandey[50] is generally accepted as the structure of the clean reconstructed diamond (111) surface.[51–55] After reconstruction, both occupied[12–14] and empty surface states[56,57] appear in the gap. While molecular hydrogen has no effect on the clean (111)-(2×1) diamond surface, room-temperature exposure to atomic hydrogen restores the surface symmetry to the original 1×1 ["rehydrogenated" (111)-(1×1):H diamond surface].[12,13] Similar to the as-polished surface, there is an absence of filled surface-state emission from the rehydrogenated surface.[13]

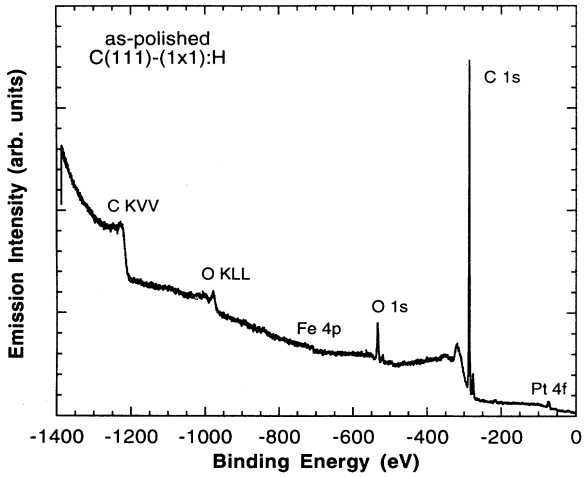

FIG. 3. XPS spectrum from the as-polished (111)-(1×1):H diamond surface. The oxygen coverage, typical of the as-polished diamond surfaces, is less than 20% of a monolayer, and the iron contamination from the cast iron polishing wheel is less than 1%. The observed platinum signal is from the clips used to mount the sample.

2. *XPS determination of surface contaminants*

An Al $K\alpha$ ($h\nu$=1486.6 eV) XPS spectrum from the as-polished diamond surface is shown in Fig. 3. Analysis of the XPS spectra finds a fraction of a monolayer of oxygen.[21,58] The oxygen coverage of the as-polished diamond surfaces that were studied was up to 20% of a monolayer. A trace (less than 1% of a monolayer) of Fe was often present, due to contamination from the cast iron wheel during polishing. The surface cleanliness of the (111)-(1×1):H rehydrogenated diamond surface was also characterized by Al $K\alpha$ XPS. In Fig. 4, we plot a typical XPS spectrum of a rehydrogenated diamond sur-

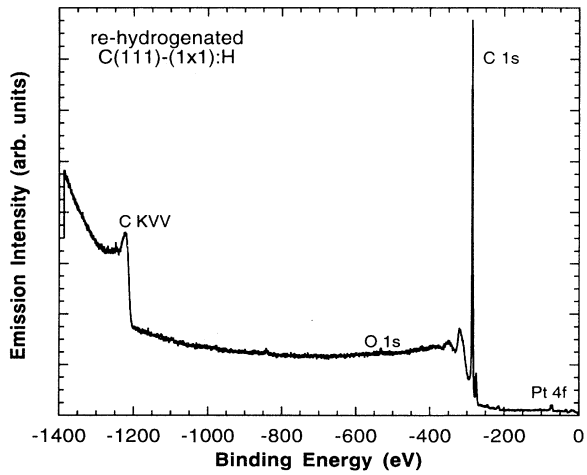

FIG. 4. Typical XPS spectrum of the rehydrogenated (111)-(1×1):H diamond surface. In contrast to the as-polished surfaces, the oxygen 1*s* peak is barely observable (less than 1% of a monolayer).

face, taken after *in situ* heating of the as-polished surface to 1000 °C and subsequent atomic hydrogen dosing. In contrast to the as-polished surfaces, the oxygen contamination of the rehydrogenated surface is reduced (less than 1% of a monolayer). The small emission feature seen in both Figs. 3 and 4, at a binding energy of 71 eV, is due to Pt 4*f* emission from the platinum sample mount.

3. *UPS characterization of band bending*

The energy position of the VBM at the surface relative to the Fermi level was determined using UPS. Valence band UPS is a surface sensitive technique due to the short inelastic mean free path [$\lambda \approx 5$ Å (Refs. 13 and 53) or less[54]] of hot electrons in diamond. Typical UPS spectra of the as-polished surface for both $h\nu = 21.2$ and 40.8 eV are shown in Fig. 5. The Fermi-level position was determined from the photoemission spectrum of the platinum foil sample mounting. It can be seen from Fig. 5 that the position of the valence-band maximum at the surface (E_V^S) of the as-polished diamond is 0.4 eV below the Fermi level. Note the feature marked with an "*A*" in the $h\nu = 40.8$ eV EDC (dotted curve, Fig. 5) lies at a binding energy of 12.8 eV below the VBM. The binding energy of the "*A*" peak is consistent with earlier experimental results,[13] and with the theoretical density of states reported by Painter, Ellis, and Lubinsky.[59] In Table I, we summarize the energies of the features discussed above and compare to earlier work.[13] The high emission intensity peak in the 21.2 eV distribution (solid curve, Fig. 5) lies at an energy corresponding to a conduction-band-minimum final state and is often cited[11,15] as indication that the surface exhibits negative electron affinity.

In Fig. 6, we compare the 21.2 eV UPS spectra from the as-polished, reconstructed and rehydrogenated diamond surfaces. Compared to the as-polished (111)-(1×1):H diamond surface (see Table I), the features

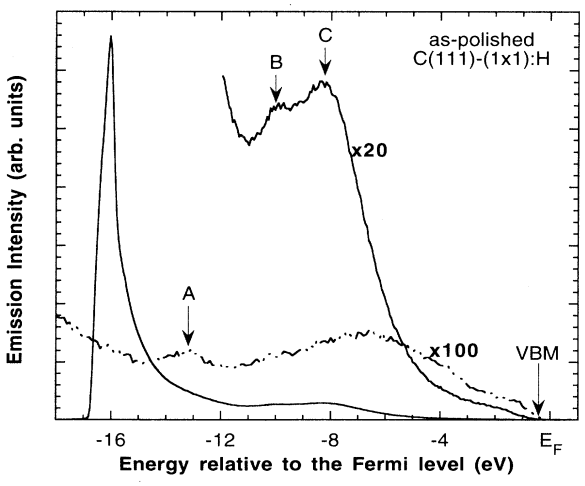

FIG. 5. Photoemission electron energy distribution curves from negative-electron-affinity, as-polished, (111) diamond surface (sample *D*5), for excitation photon energies 21.2 eV (solid line), and 40.8 eV (dotted line).

TABLE I. Summary of the binding energies of the VBM, and *A*, *B*, and *C* features from Fig. 5 ("This work"). We also show the corresponding energies as determined from Fig. 15 of Pate (Ref. 13).

		A	*B*	*C*	VBM at the surface (E_V^S)
$E-E_F$ (eV)	This work	−13.2	−10.0	−8.2	−0.4
	Pate[a]	−13.6	−10.4	−8.5	−0.8
$E-E_V^S$ (eV)	This work	−12.8	−9.6	−7.8	
	Pate[a]	−12.8	−9.6	−7.7	

[a]Reference 13.

A (−14.0 eV) and *C* (−9.0 eV) in the energy distribution curve of the reconstructed surface have both shifted 0.8 eV towards lower kinetic energies. This reflects a change in the band bending, due to a change in surface Fermi-level pinning position. Upon rehydrogenation, the bands shift 0.2 eV upwards. We were unable to reproduce the Fermi-level pinning position of the as-polished diamond surface by rehydrogenating the reconstructed surface. The irreversibility of the Fermi-level pinning position has been previously observed[53] and is likely due to incomplete hydrogenation,[60] which leaves a small concentration of surface states in the gap. The reconstructed surface exhibits a filled surface-state band[13,14] with a bandwidth of about 2 eV [see inset in Fig. 6 (Ref. 61)] and centered at 2.4±0.2 eV below the Fermi level. The

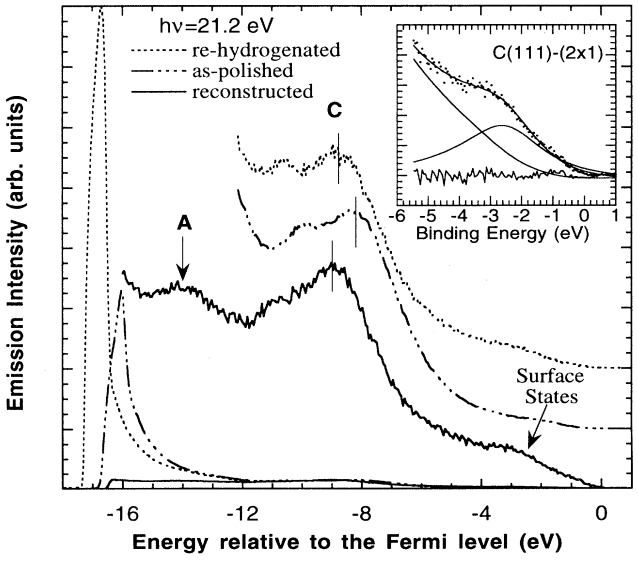

FIG. 6. Electron energy distributions of the as-polished, reconstructed and rehydrogenated (111) diamond surfaces. In contrast to the reconstructed surface, both as-polished and rehydrogenated diamond surfaces exhibit negative electron affinity.

TABLE II. Position of the VBM and surface states in (111) diamond surfaces.

Sample	Type	as-polished $E_F-E_V^S$ (eV)	Reconstructed $E_F-E_V^S$ (eV)	Rehydrogenated $E_F-E_V^S$ (eV)	Surface states $E_V^S-E_{SS}$ (eV)
$D3$[a]	IIa	0.8			
$D4$[a]	IIb	0.6	1.35		
$D4$[a]	IIb	0.7	1.2	1.2	1.1
$D5$[b]	IIb	0.4	1.2	1	1.2
Himpsel *et al.*[c]	IIb	1 (cleaved in H)	1.5		1
van der Weide *et al.*[d]	IIb	0.8	1.6		1.2

[a]Reference 13.
[b]Present work.
[c]Reference 14.
[d]Reference 62.

surface-state peak lies at 1.2 eV below the valence-band maximum, in agreement with others[12,14,62] (see Table II).

The emission width, W, from the low-kinetic-energy cutoff to the VBM emission can be used to calculate the electron affinity, using $\chi=h\nu-E_g-W$ (see Sec. II A). In the case of the reconstructed surface, the emission width is $W=15.2$ eV, resulting in a positive electron affinity $\chi=+0.5$ eV. The same calculation for either of the hydrogenated surfaces finds $\chi<0$. In Table II, we tabulate the observed values of the position of the VBM at the surface E_V^S with respect to the Fermi level, and the energy shifts due to band bending between the as-polished, rehydrogenated and reconstructed (111) diamond surfaces, along with the position of surface states with respect to the VBM. Note that $E_F-E_V^S$ is an extrinsic value and can differ between samples depending upon bulk doping and surface treatment.

To better understand the band bending, we need knowledge of the bulk Fermi-level position. It is known that the acceptor center in natural semiconducting diamond is boron,[63,64] with an ionization energy of $E_A=0.365$ eV.[64,65] By requiring charge neutrality, we can calculate[66] the bulk Fermi-level position of boron-doped diamond as a function of the temperature and the impurity concentration. We tabulate the room-temperature bulk Fermi-level position with respect to the VBM for a range of boron impurity concentrations in Table III. In so doing, we have used the electron effective masses reported by Nava *et al.*,[34] and the hole effective masses reported by Kono *et al.*[33] The dependence of the band gap on temperature [$E_g=5.4925+1.979.10^{-4}T^2/T-1437$ eV (Ref. 67)] has also been taken into account.[40] If one assumes complete acceptor ionization, then the width (D) of the band bending region can be calculated from $D=\sqrt{2\varepsilon\psi/qN_A}$,[66] where ε is the dielectric constant, ψ is the band bending potential in volts, and N_A the acceptor density. In Table III, we derive the band bending potential, ψ, from the difference of the calculated bulk Fermi-level position with respect to the bulk VBM, to the experimentally determined Fermi-level position with respect to the VBM at the surface. For typical boron concentrations in natural type-IIb diamonds [$10^{14}-10^{16}$ cm^{-3} (Ref. 68)], the band bending is long with respect to the characteristic path length for photon thermalization. In addition, since the acceptors are not completely ionized, the characteristic band bending width has been underestimated, more severely underestimated at the higher doping concentrations. Furthermore, since the accuracy of the surface VBM determination is no better than ±0.1 eV, the UPS

TABLE III. Bulk Fermi-level positions, band bending, and band bending lengths of the as-polished (111):H diamond surface are tabulated. The last column represents the band bending length assuming completely ionized acceptors. The effect of incomplete ionization is to increase the band bending lengths at higher ($\geq 10^{14}$ cm^{-3}) doping levels. When there is upwards ($\psi<0$) band bending to the surface (e.g., $N_a=10^{12}$ cm^{-3}), the band bending length is set by unknown compensating donors. Note that the uncertainty in surface Fermi-level energy position ($E_F-E_V^{\text{Surf}}$) is sufficient to be consistent with upward band bending within the likely range of acceptor density (10^{14}–10^{16} cm^{-3}).

Acceptor density N_a (cm^{-3})	Ionized bulk dopant (%)	Calculated $E_F-E_V^{\text{bulk}}$ (eV)	as-polished $E_F-E_V^{\text{Surf}}$ (eV)	as-polished $\psi=E_V^{\text{bulk}}-E_V^{\text{Surf}}$	Estimated length $D=\sqrt{2\varepsilon\psi/qN_A}$ (Å)
10^{12} cm^{-3}	95%	0.44 eV	0.4±0.1 eV	−0.04 eV	?
10^{14} cm^{-3}	46%	0.36 eV	0.4±0.1 eV	0.04 eV	4800 Å
10^{16} cm^{-3}	7%	0.30 eV	0.4±0.1 eV	0.10 eV	700 Å
10^{18} cm^{-3}	<1%	0.24 eV	0.4±0.1 eV	0.16 eV	100 Å

measurements, and expected dopant concentrations, are consistent with either upward or downward band bending. Note that under the conditions cited in the table, an acceptor density of 10^{12} cm^{-3} results in upward band bending. In that case the band bending length is determined by unknown compensating donors, and would likely be characterized by a very long band bending length (due to the expected small donor concentration).

B. Photoelectric threshold structures ($h\nu \leq 5.57$ eV)

The characteristic photoabsorption penetration depth, $1/\alpha$, of diamond is shown in Fig. 7 for excitation photon energies between 5 and 30 eV. The solid line was determined from transmission measurements of thin single-crystal fragments by Clark, Dean, and Harris.[29] The dotted line is a calculation[69] of the adsorption coefficient from the real and imaginary parts of the dielectric constant, as determined by Roberts and Walker,[70] using reflectivity techniques. As can be seen in Fig. 7, the characteristic absorption length at threshold photon energies ($h\nu \leq 5.57$ eV) exceeds tens of micrometers. In such a case, the characteristic penetration depth $1/\alpha$ greatly exceeds the likely carrier diffusion length L, and the three-step model, Eq. (5), reduces to

$$Y(h\nu) \cong P_{ex} L_{ex} \alpha_{ex}(h\nu) + P_{el} L_{el} \alpha_{el}(h\nu) \ . \quad (6)$$

In this case, each component of the photoelectric yield is proportional to the respective component of the adsorption coefficient.

In Fig. 8 we compare the absorption coefficient ($T = 100$ K spectra from Ref. 29) at threshold with the measured total electron yield (large dots) from the as-polished (111)-(1×1):H diamond surface, at 130 K. Note

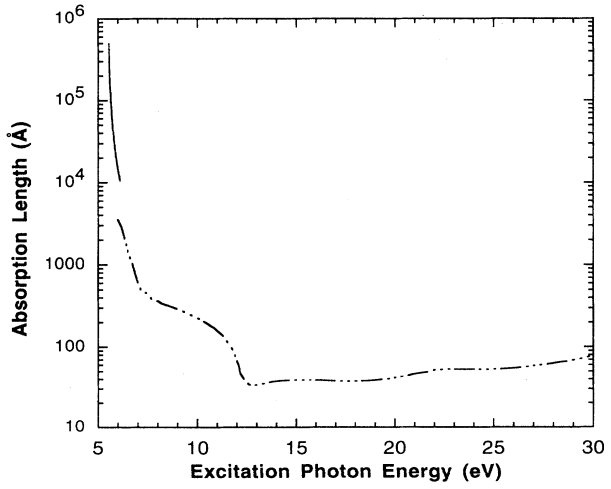

FIG. 7. The characteristic photoabsorption length in diamond. Note that at photon energies near threshold, the absorption length is very long (of the order of hundreds of micrometers or longer).

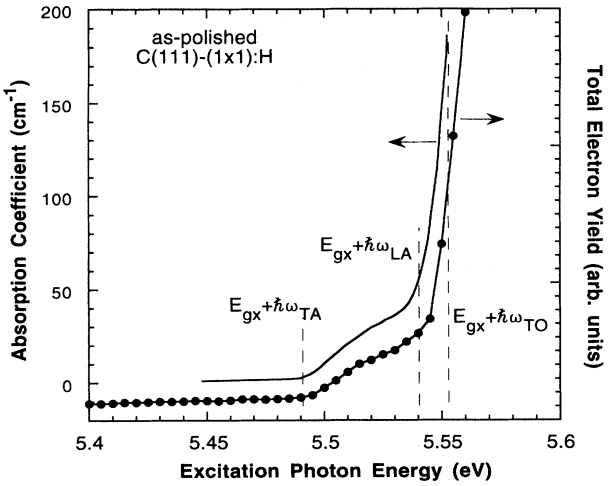

FIG. 8. (. . . .) Total electron yield at 130 K, and (——) absorption edge spectrum at 100 K from Clark, Dean, and Harris (Ref. 29). The dashed lines correspond to the photoabsorption thresholds (Table IV), as discussed by Clark, Dean, and Harris. In this energy range and at these temperatures, photoexcitation occurs via phonon emission to exciton levels only. Therefore, the similarity between the electron yield and the absorption coefficient implies that the observed electron emission is derived solely from dissociation of bound electron-hole pairs.

that for presentation purposes, the zero of the absorption coefficient has been shifted upwards. Consistent with Eq. (6) above, the measured electron yield from negative-electron-affinity diamond is found to be in close agreement with the photoabsorption coefficient. The energy thresholds as determined by Clark, Dean, and Harris[29] for photoabsorption to Mott-Wannier exciton final states via phonon emission are tabulated in Table IV and also marked in Fig. 8 with dashed lines. The lowest-energy threshold for creation of *unbound* electron-hole pairs is $h\nu = 5.57$ eV ($h\nu - \hbar\omega_{TA} = E_g$), which lies outside the range of the data shown in Fig. 8. Therefore, since $\alpha_{el}(h\nu) = 0$ for $h\nu < 5.57$ eV, the second term of Eq. (6) is zero. Based upon (a), the similarity between the absorption coefficient and total electron yield spectra from the NEA (111) diamond surfaces (Fig. 8), and (b), and the fact that for $h\nu < 5.57$ eV photoexcitation occurs only to exciton states ($T = 130$ K), we can conclude that the observed electron emission is derived solely from *bound* electron-hole pairs *(Mott-Wannier excitons)*. Further analysis (see below) finds that the exciton dissociation event that leads to electron emission occurs at the diamond-vacuum interface.

C. The form of the photoelectric yield ($5.57 \leq h\nu \leq 6.1$ eV)

1. The as-polished hydrogenated surface

The total photoelectron yield (solid lines) from the as-polished negative-electron-affinity (111)-(1×1):H dia-

TABLE IV. Absorption thresholds that correspond to photoexcitation with simultaneous phonon emission from Clark, Dean, and Harris (Ref. 29).

Threshold assignment by Clark, Harris, and Dean[a]	Threshold energy (eV) at 295 K	Threshold energy (eV) at 130 K
(1) $E_{gx}+(\hbar\omega)_{TA}$	5.482±0.002	5.491
(2) $E_{gx}+(\hbar\omega)_{LA}$	5.531±0.002	5.540
(3) $E_{gx}+(\hbar\omega)_{TO}$	5.544±0.002	5.553

[a] $E_{gx}=E_g-E_x=5.4$ (eV), $(\hbar\omega)_{TO}=143$ meV, $(\hbar\omega)_{TA}=83$ meV, $(\hbar\omega)_{LA}=132$ meV. The room-temperature assignments and threshold energies are taken directly from Table I of Clark, Dean, and Harris (Ref. 29). The 130 K thresholds are derived from the 295° K thresholds by including the temperature dependence (Ref. 67) of the band gap.

mond surface, both at 295 and 130 K, is shown in Fig. 9 for excitation photon energies between 5 and 6.1 eV. Consistent with previous observations,[71] the total electron yield is found to exhibit an oscillatory structure as a function of the excitation photon energy. The oscillations, which do not appear in the absorption coefficient,[29] are approximately evenly spaced with a 160-meV period. The oscillatory structure becomes more pronounced, and there is a striking increase in the total electron yield as the sample temperature is lowered.

Using Eq. (5), the photon energy dependence of the total electron yield from the as-polished (111)-(1×1):H diamond surface (both at 295 and 130 K) can be reproduced

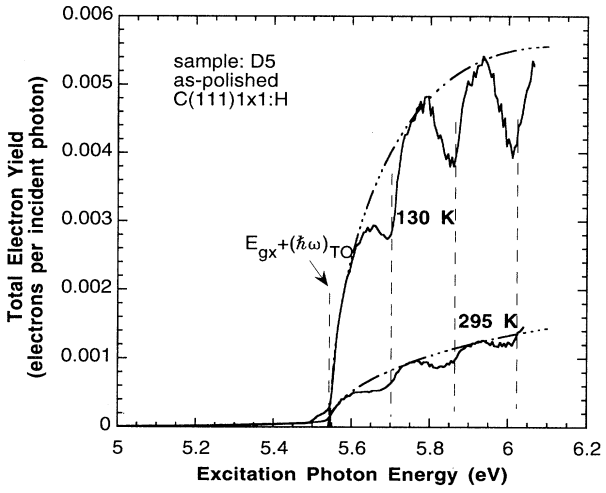

FIG. 9. Total electron yield vs excitation photon energy at 130 and 295 K, from the as-polished (111)-(1×1):H NEA diamond surface (solid line). Predicted functional form of the total electron yield (· · · ——) according to Spicer's three-step model with the assumption that only the exciton component contributes to the emission. Note that the oscillations in photoelectric yield are evenly spaced by approximately 160 meV. The lowest-energy threshold lies at a photon energy that corresponds to excitation from the valence-band maximum to the exciton ground state via TO-phonon emission.

from the absorption coefficient, by assuming that the exciton producing component $[\alpha_{ex}(h\nu)=A(h\nu-5.54)^{0.5}]$ dominates. This has been done (· · · — in Fig. 9) by assuming that P_{ex} and L_{ex} are independent of $h\nu$ and taking the values of $\alpha(h\nu)$ and $\alpha_{ex}(h\nu)$ from Clark, Dean, and Harris[29] [Eq. (3)]. For the fit in Fig. 9, we chose the values of L_{ex} to be 1000 Å at 295 K and 5300 Å at 130 K, while fixing P_{ex} ($P_{ex}=0.0736$). Except for periodic dips in the electron yield, there is striking agreement between the functional form of the total photoelectron yield and the three-step model, Eq. (5), assuming only exciton-derived emission. Within this model, the increase in electron yield as the temperature is lowered results from a fivefold increase in the diffusion length of the exciton. The observed temperature dependence is, therefore, consistent with exciton diffusion lengths governed by exciton-phonon scattering (i.e., an intrinsic property) and not extrinsic (e.g., impurity) scattering.

Above $h\nu=5.8$ eV, the strongest component of the total photoabsorption is the excitation of valence-band electrons into *unbound* electron-hole pair states (free conduction-band electrons).[6,29] However, as evidenced by their absence in the electron yield excitation spectra (Fig. 9), photoexcited electrons derived from this absorption component are not emitted. Regardless of the transport and/or escape mechanism responsible for the lack of conduction-band electron emission, the absence of the emission suggests that bulk conduction-band electrons, including those which might be produced as an exciton decay product (e.g., exciton ionization), do not significantly contribute to the electron emission. Therefore, we conclude that the exciton-derived emission *must result from exciton dissociation at the diamond-vacuum interface.* Otherwise, in contrast to the observed total electron yield, one would expect electron emission due to photoproduction of both excitons and conduction-band electrons.

2. *The in situ rehydrogenated surface*

Total electron yield spectra from the rehydrogenated diamond surface both at room temperature (295 K) and

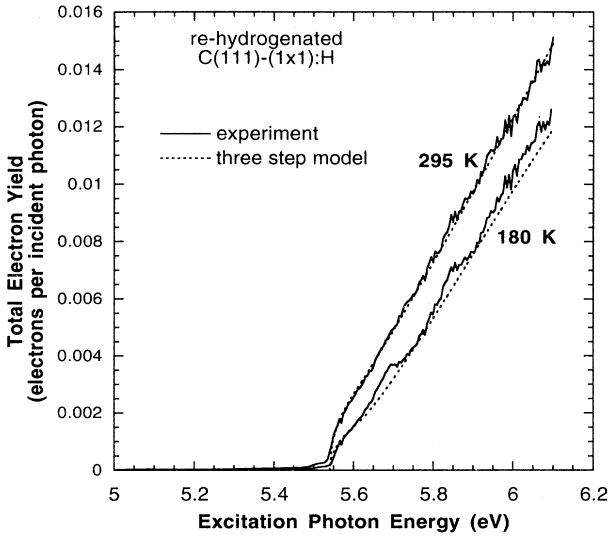

FIG. 10. Total electron yield from the rehydrogenated (111)-(1×1):H diamond surface, both at room temperature (295 K) and 180 K (solid lines). With dotted lines, we show the calculated functional form, Eq. (5), of the total electron yield, using the three-step model.

180 K are shown in Fig. 10. In contrast to the as-polished surface, the rehydrogenated (111)-(1×1):H diamond surface exhibits oscillatory photoelectric emission only at low temperatures. As before, we use Spicer's three-step model for photoemission[5] [see Eq. (5)] to model the observed total electron yield from the rehydrogenated negative-electron-affinity (111) diamond surface. In contrast to the as-polished diamond surface, satisfactory fit to the data from the rehydrogenated surface can only be achieved by assuming that both photoexcited excitons *(bound* electron-hole pairs) and conduction-band electrons *(unbound* electron-hole pairs) contribute to the electron yield. Recall that the principle physical difference between the as-polished and rehydrogenated surfaces is the change in band bending from nearly flat band to definite downward band bending.

Assuming that both P's and L's are independent of $h\nu$, the functional form of the total electron yield from the rehydrogenated surface (both at 295 and 180 K) can be reproduced quite closely (· · · · in Fig. 10) from the three-step model, Eq. (5). For the fits presented in Fig. 10, we chose at 295 K, $L_{ex}=1000$ Å (as in the case of the as-polished diamond surface), $P_{ex}=0.386$, $L_{el}=1050$ Å, $P_{el}=0.107$, and at 180 K, $L_{ex}=2400$ Å, $P_{ex}=0.092$, $L_{el}=4000$ Å, $P_{el}=0.038$. Due to the fact that the denominators in Eq. (5) vary slowly compared to the numerators, the above values are not accurate estimates of the P's and L's. Even so, the striking agreement between the functional form of the total electron yield and the model used to derive the fits leads us to conclude that the observed electron emission originates from both photoexcited excitons and conduction-band electrons.

3. *Field ionization of excitons*

In a sufficiently large electric field, excitons will ionize and become an *unbound* electron-hole pair. It is well known that there are large electric fields in semiconductors, especially near surfaces, due to band bending. Here, we consider the field requirements for exciton ionization in diamond and compare to the built-in electric fields (due to band bending) that occur in our samples. As a guide to the required field for exciton ionization, we consider the ionization field of a hydrogen atom (2 V/Å).[72] The exciton binding energy (80 meV) in diamonds is 170 times smaller than the H ground state (13.6 eV) and the diamond dielectric constant is $\varepsilon=5.7$. The smaller binding energy, together with the more extended state (due to the dielectric screening of the solid) act to reduce the required ionization field as compared to the hydrogen atom. Therefore, an estimate of the electric-field sufficient to field ionize an exciton in diamond is given by 0.002 V/Å (=2 V/Å/170×5.7). Assuming a parabolic band bending region, the electric field will increase linearly as we approach the semiconductor-vacuum interface, and its maximum value will be $2\psi/D$,[66] where ψ is the magnitude of the band bending at the surface in volts, and D is the width of the band bending region.

Consider the rehydrogenated surface, with an assumed bulk doping density of 10^{16} cm^{-3} (on the high side of the acceptor densities observed in natural type-IIb diamond). Using results from Sec. IV A 2, there is 0.7 eV downward band bending and a band bending length of $D=2000$ Å. We, therefore, find that the field, due to band bending at the rehydrogenated diamond surface, is ~0.0007 V/Å. Using the same bulk doping, we find that the maximum field at the as-polished surface is ~0.0003 V/Å (ψ and D from Table III). A more reasonable estimated bulk doping ($<10^{16}$ cm^{-3}) reduces the maximum estimated field. These results are consistent with the survival of the excitons as they traverse the band bending region of either the as-polished or rehydrogenated surfaces.

D. Electron energy distributions

1. *The as-polished hydrogenated surface*

The kinetic energy distributions of photoelectrons emitted from the as-polished diamond surface at room temperature for a variety of near-band-gap excitation photon energies have been previously discussed.[6] The distribution curves were found to be broad (0.6 eV FWHM), with emission energies that lie within the band gap of diamond. The emission at energies below the CBM was argued to be due to exciton-derived emission. In Fig. 11 we plot, for comparison, the electron energy distributions from the as-polished (111)-(1×1):H diamond surface, both at room temperature and 180 K for excitation photon energy 6.065 eV. The energy distributions have been normalized to the same height and shifted vertically for presentation purposes. As can be seen, the energy distribution is found to become somewhat more narrow (~0.5 eV FWHM) and more asymmetric as the temperature is lowered. It appears that the low-

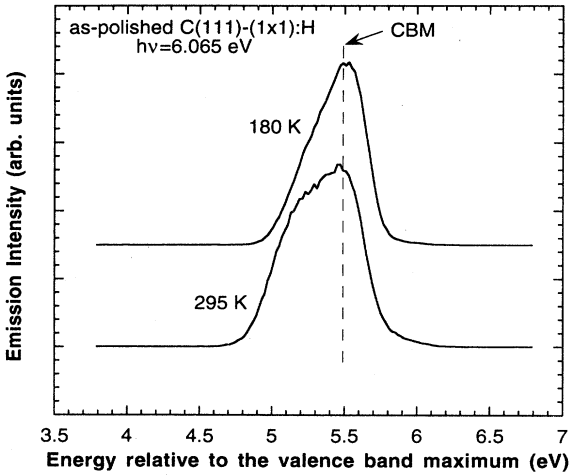

FIG. 11. Electron energy distribution curves referenced to the valence-band maximum at the surface, for 6.065 eV excitation photon energy, both at room temperature and 180 K from the as-polished (111)-(1×1):H diamond surface.

energy side of the low-temperature EDC has relatively lower intensity, which could be due to a slight change of the electron affinity. Furthermore, there is no shift of the energy distribution as we lower the temperature. The absence of temperature-dependent energy shifts of the EDC's is consistent with flat energy bands at the surface (band bending <0.1 eV) and suggests that no photovoltaic effects are present.[73,74]

2. *The in situ rehydrogenated surface*

Room-temperature EDC's from both rehydrogenated and as-polished diamond surfaces for excitation photon energy of 6.065 eV are compared in Fig. 12. These energy distribution curves are normalized to the same height

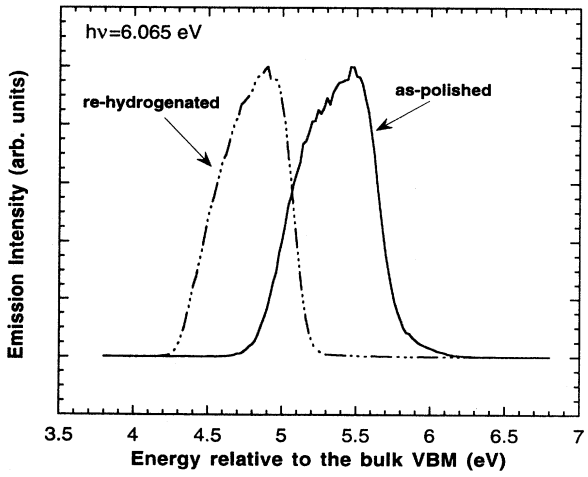

FIG. 12. Comparison between the $h\nu=6.065$ eV EDC's (referenced to the bulk VBM) of the as-polished and rehydrogenated diamond surfaces at room temperature. In this figure, we have assumed that $E_F-E_V^{\text{Bulk}}=0.4$ eV.

for presentation purposes. Consistent with the 21.2 eV UPS data (Fig. 6), the ~ 0.6 eV shift to lower energies of the EDC from the rehydrogenated diamond surface (Fig. 12) is due to the additional (compared to the as-polished surface) downward band bending. For 0.7 eV downwards band bending, and typical acceptor densities in natural diamond ($10^{14}-10^{16}$ cm^{-3}), the width of the band bending region is expected to be between 2000 and 20 000 Å.[66] Note that the width and shape of the electron energy distributions from the nearly flat-band surface (as-polished) and from the downward band bending surface (rehydrogenated) are very similar. This leads us to conclude that band bending is not responsible for the broad emission width. This result is consistent with the expectation that carriers thermalize in a distance that is short (of the order of 100 Å or less), as compared to the long (2000 to 20 000 Å) band bending region, and reach the surface at thermal ($\sim kT$) energies. These results suggest that the broad energy width of emission is related to common escape step (whether exciton-derived or CB electron derived).

E. Oscillations in the photoelectric yield

1. *The as-polished hydrogenated surface*

We now turn to the distinct oscillatory structure (Fig. 9) in the photoelectric emission from the as-polished diamond surface. The oscillations, which were observed first by Pate, Lindau, and Spicer[71] are evenly spaced with about 160-meV period. In their attempt to explain the oscillatory structure, the Frank-Condon principle was applied to model the mechanism responsible for the oscillations. Although there is a phenomenological agreement between the oscillator strengths of the multiplet, which result from application of the Frank-Condon principle, and the yield oscillatory structure, the lack of any similar oscillatory structure in the absorption coefficient of diamond suggests that the observed oscillations cannot be due to a variation in photoabsorption.[75] Therefore, the phenomenological model that was presented[71] cannot be responsible for the electron yield oscillations.

Strong exciton-phonon coupling is expected for small radius excitons, due to the dependence of exciton energy on the inter-atomic interaction, which in turn is sensitive to lattice distortion.[76] Typical intraband exciton-phonon scattering lifetimes of semiconductors are of the order of $10^{-11}-10^{-13}$ sec.[26,77] In contrast to direct-gap materials, the indirect band gap of diamond results in long exciton recombination lifetimes. Typical recombination lifetimes for indirect excitons are from microseconds to milliseconds, while for direct excitons, the equivalent lifetimes are about 1 nsec.[78] Therefore, excitons in diamond are expected to thermalize, via phonon emission, in very short times relative to their recombination lifetime. The dashed lines in Fig. 9 mark the excitation photon energies that result in hot excitons, which can thermalize to the exciton band minimum via emission of 160-meV phonons (phonon cascade[6]), in a way similar with the Fan model.[79] The oscillations in the total electron yield correspond to oscillations in the flux of excitons that reach the surface

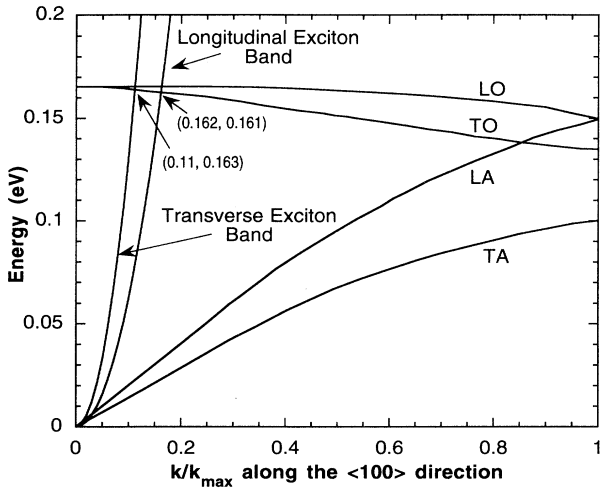

FIG. 13. Phonon-dispersion curves (Ref. 22) and parabolic exciton bands in diamond ($M_{\text{long}}=1.9m_0$, $M_{\text{trans}}=0.9m_0$). Transverse-optical phonons with the right wave vector to participate in a phonon-cascade mechanism have energies of about 160 meV, which is in good agreement with the observed oscillations in the total electron yield.

to emit their electrons into the vacuum.[6]

In order for a Fan-type phonon-cascade mechanism to be operative, the existence of phonon states with the correct energy at the required wave vector is necessary. In Fig. 13, we plot the exciton band dispersion, which we assume to be parabolic (see discussion in Sec. II C) and the phonon dispersion.[22,80] The intersection of the dispersion curves indicates that the required (E,k) conditions are met by TO phonons for the final step in the TO-phonon cascade to the exciton band minimum. Due to the relatively flat optical-phonon bands near the zone center (see Fig. 13), TO phonons involved in scattering of excitons high in the band are quasimonochromatic with the final TO-phonon cascade step. Therefore, examination of the phonon band structure of diamond indicates that TO-phonon scattering is consistent with the proposed phonon-cascade mechanism.

In Fig. 14(a) we plot constant final-state spectra, for electron kinetic energies, E, less than ($E=4.9$ eV with respect to the VBM) and equal to the exciton-band minimum (EBM) ($E=5.4$ eV, with respect to the VBM). Both spectra exhibit an oscillatory structure, and when normalized to the same intensity, the oscillations have approximately the same strength. In contrast, the oscillatory structure in the constant final-state spectra becomes less pronounced as the final-state energy is increased [Fig. 14(b)] above the conduction-band minimum (5.5 eV). At a final-state energy of 5.85 eV, the yield no longer oscillates, and resembles the expected photon energy dependence of the absorption coefficient component, which produces *unbound* electron-hole pairs.[6,29] In summary, the constant final-state spectra demonstrates that the oscillatory photoyield from as-polished diamond (111) is due to a uniform oscillation, in the emission intensity of the broad emission feature within the band gap (see Fig. 11).

2. *The in situ rehydrogenated surface*

Unlike the as-polished surface, the rehydrogenated (111)-(1×1):H diamond surface exhibits observable oscillatory structure only at low temperatures (Fig. 10). The oscillations are weaker and out of phase with the yield oscillations from the as-polished diamond surface. That is, maxima occur at excitation photon energies that correspond to minima in the as-polished diamond surface yield spectra. We note that at room temperature, our three-step model analysis (see IV C 2) finds that the electron and exciton diffusion lengths are approximately equal to each other ($L_{\text{ex}}\approx L_{\text{el}}$), while at 180 K $L_{\text{el}}>L_{\text{ex}}$. This result is consistent with the out-of-phase oscillations in the total electron yield from the rehydrogenated surface at 180 K. The dips (oscillation) in the total electron yield from the as-polished surface are due to the turn on of an exciton ionization mechanism.[6] Once the exciton is ionized, the exciton population is diminished, while at the same time producing an unbound electron-hole pair. The population of conduction-band-minimum electrons is, therefore, expected to exhibit oscillations which, in comparison to the exciton population, are out of phase. The particular oscillations that we observe (whether "in phase" or "out of phase") depends upon which component (exciton or conduction-band-minimum electrons)

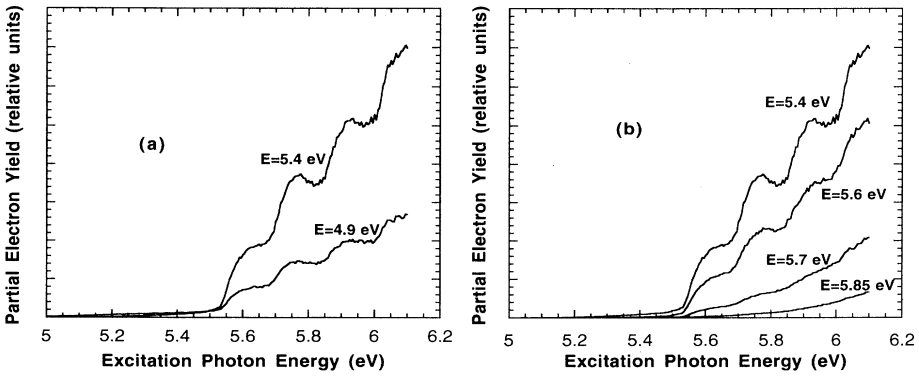

FIG. 14. Constant final-state curves from the as-polished (111) diamond surface. The kinetic energy (E) of the electrons is with respect to VBM (Fig. 12). (a) $E\leq$EBM, the partial yield oscillates uniformly as the final-state energy, E, is lowered. (b) $E\geq$EBM, the oscillations become less pronounced as the final-state energy, E, is increased.

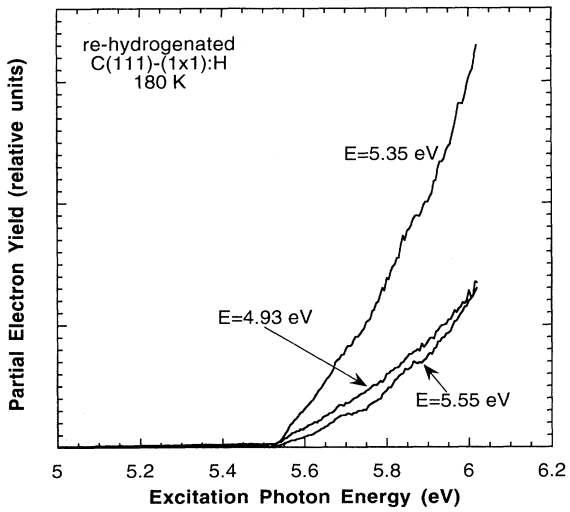

FIG. 15. Constant final-state curves from the rehydrogenated (111) diamond surface. The kinetic energy (E) of the electrons is shown with respect to the bulk valence-band maximum (see Fig. 12). The observed oscillatory structure is due to flux variation of the conduction-band electrons that reach the diamond-vacuum interface.

dominates. At low temperatures, we observe the out-of-phase oscillatory structure in the total electron yield from the rehydrogenated surface (Fig. 10), since, relative to excitons, electrons are more efficient ($L_{el} > L_{ex}$) in reaching the diamond-vacuum interface. At room temperature ($L_{ex} \approx L_{el}$) no oscillations are observed, due to the fact that both excitons and conduction-band electrons reach the surface and escape with comparable efficiency. In Fig. 15, we show constant final state spectra from the rehydrogenated (111) diamond surface at 180 K. In contrast to the as-polished diamond surface, the out-of-phase oscillatory structure is stronger in the constant final-state spectra of the most energetic electrons. This result supports our assignment that the out-of-phase oscillations are due to variation in the flux of the conduction-band-minimum electrons (a product of exciton dissociation) that reach the diamond-vacuum interface.

F. Transport and escape mechanisms

Clearly, in the case of the as-polished diamond (111) surface, there is a transport or escape mechanism, which is acting to quench the electron emission of conduction-band-minimum electrons. We find that upward band bending is the simplest mechanism that could be responsible. Upward band bending at the surface produces an electric field that repels conduction-band electrons, yet has little effect on uncharged carriers such as excitons. In this way, upward band bending can act to selectively "turn off" the transport of conduction-band electrons to the surface without altering exciton transport. As discussed in IV A 3, the existence of upward band bending at the as-polished (111)-(1×1):H surface is consistent with the likely range of acceptor densities and with the uncertainty of the UPS measurements. Furthermore, the disappearance (and reversal at low temperatures) of the spectral oscillations with the change in band bending is consistent with this simple band bending argument for the absence of significant conduction-band electron emission from the as-polished surface. In support of this argument, experiments made on the diamond (111):TiO surface,[17] which find a downward band bending similar to that found at the rehydrogenated diamond surface, produce photoelectric yield properties that are essentially identical to those of the rehydrogenated surface.

The form of the negative electron affinity of diamond (111)-(1×1):H (whether *true* or *effective)* would have some bearing on the electron escape probability for exciton-derived or electron-derived electron emission. Qualitatively consistent with quantum chemistry studies of hydrocarbon fragments,[81] which find *true* (band bending is not an issue) NEA, with experimental studies of long chain hydrocarbons[82] that find *true* NEA, and with *ab initio* local-density-based theoretical determination of *true* NEA for C(100)-(2×1):H,[9] our finding that the as-polished NEA (111)-(1×1):H surface is nearly flat band argues strongly for the existence of *true* negative electron affinity.

The indirect band gap of diamond can have implications on the escape probability of electron emission from the (111) surface.[83] A simple electron escape model of emission from a perfect surface requires, in addition to conservation of energy, conservation of the component of the electron wave vector, which is parallel to the emission surface ($\mathbf{k}_{\parallel}$).[84,85] We have analyzed[6] this constraint and find that χ must be less than -4.55 eV in order to allow for wave-vector conserving electron escape. In this case, the wave vector of the emitted electrons has a large $\mathbf{k}_{\parallel}$ component, which implies [due to (111) surface symmetry] a distinct threefold azimuthal angular distribution of emission, with little intensity directed along the surface normal. However, the angular distribution of the observed emission, Fig. 16, is directed along the surface

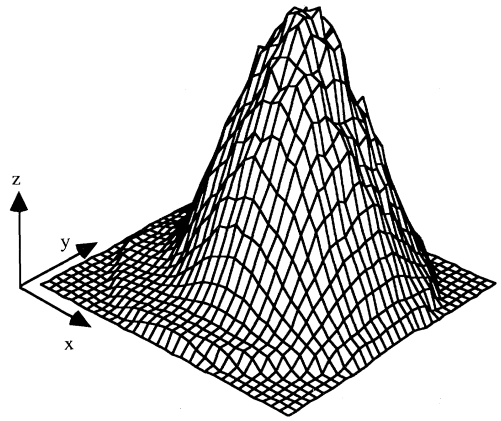

FIG. 16. Angular distribution of the emitted electrons ($h\nu = 5.69$ eV). The distribution is directed along the surface normal with a broad (70° FWHM) angular width and cylindrical symmetry. The vertical scale indicates the number of counts arrived at the x,y, position of the detector.

normal with a broad (70° FWHM) angular width and cylindrical symmetry. This experimental result indicates that a more complicated escape mechanism is involved. Extrinsic effects, such as surface roughness, could play an important role in the emission phenomena.

Higher-order processes, such as phonon-assisted emission, can remove the requirement ($\chi < -4.55$ eV) that the magnitude of the negative electron affinity be large. Because of the dipole nature of the surface-vacuum interface and the polar nature of the electron-hole pair, it is reasonable to expect strong exciton-lattice coupling, which results in phonon emission during exciton breakup at the surface. Likewise, the Coulomb interaction of the electron with the polar surface could produce electron-lattice coupling. Electron-emitting exciton breakup then becomes a many-body problem with emission of not only a free electron, but also multiple phonons and a hot hole. In this case, energy (E) and wave vector ($\mathbf{k}_{\parallel}$) conservation arguments for the exciton can be written as

$$E_{\text{exciton}} \pm E_{\text{phonon}} = E_{\text{electron}} + E_{\text{hole}} , \tag{7}$$

$$\mathbf{k}_{\parallel}^{\text{exciton}} \pm \mathbf{k}_{\parallel}^{\text{phonon}} = \mathbf{k}_{\parallel}^{\text{electron}} + \mathbf{k}_{\parallel}^{\text{hole}} , \tag{8}$$

and for the electron as

$$E_{\text{CBM-electron}} \pm E_{\text{phonon}} = E_{\text{electron}} , \tag{9}$$

$$\mathbf{k}_{\parallel}^{\text{CBM-electron}} \pm \mathbf{k}_{\parallel}^{\text{phonon}} = \mathbf{k}_{\parallel}^{\text{electron}} . \tag{10}$$

The qualitative effect of a complex many-body final state is (as in nuclear β decay[86]) to produce a broad kinetic-energy distribution of the emitted particle, due to the variety of accessible final states of the system. As discussed earlier (Fig. 12), both exciton-derived and electron-derived emission are in the form of a broad electron energy distribution. Assuming that the complex escape step is responsible for the broad energy distribution leads to the conclusion that the vacuum level lies at the low-energy threshold of the EDC's, namely, 0.7 eV below the CBM (see Fig. 11).

V. CONCLUSIONS

Study of the electron emission properties of negative-electron-affinity diamond surfaces finds that exciton-derived electron emission is a significant component of the observed total electron yield for near-band-gap excitation photon energies. Exciton-derived emission is the dominant component of the photoelectric yield from the as-polished diamond (111) surface. We have demonstrated that surface band bending plays an important role in determining both the photon energy dependence and the intensity of the observed photoelectric emission. The as-polished surface is thought to have slight upward band bending to the surface, which forms a transport barrier for electrons, but not for excitons. Diamond (111) negative-electron-affinity surfaces, which are modified to exhibit additional downward band bending, are found to exhibit higher photoelectric emission efficiencies and have a photon energy dependence, which demonstrates that conduction-band-minimum electrons are a significant part of the total electron yield. Experiments on both the rehydrogenated (111) diamond surface and TiO-diamond (111) interface,[17] which have similar downward band bending, result in a very similar total electron yield.

Spectral oscillations in the photoelectric yield result from exciton dissociation during transport (the Fan model). Photoexcited excitons with kinetic energy in excess of the TO-phonon energy rapidly thermalize via TO-phonon emission. If the thermalized final-state kinetic energy exceeds the exciton binding energy, the exciton ionizes to become an unbound electron-hole pair. Therefore, the number of excitons and conduction-band-minimum electrons oscillate (out of phase, with respect to each other), as a function of excitation photon energy. Depending on which component of the total electron yield (excitons or conduction-band electrons) is dominant, we observe two different kinds of oscillations, which are out of phase with respect to each other. In the case of similar emission efficiencies between excitons and conduction-band electrons no oscillatory structure is observed. Partial yield (constant final state) measurements confirm this analysis with the observation of in-phase oscillations in emission at low final-state energies (in the gap), and out-of-phase oscillations at high final-state energies (above the CBM). The kinetic-energy distributions of emitted electrons become only slightly more narrow at low temperature. The broad energy width is thought to result from a coupling to the lattice via a complex escape step, which excites vibrational modes and, in the case of exciton-derived emission, produces a hot hole.

Diamond is far from the only wide band-gap material that can be prepared to exhibit *true* negative electron affinity. For example, Benjamin *et al.*[87,88] have reported *true* negative electron affinity of AlN. In addition, many rare-gas solids[89] and some alkali halides[90] are thought to have *true* negative electron affinity. Electron energy distributions from LiF (Ref. 90) find emission in the gap, similar to our result from diamond. Related studies of positronium (an exciton analog) in rare-gas solids find that the threshold for positron activated electron emission coincides with positronium formation, and not electron-hole pair production.[91] As a consequence of our work, it is clear that mobile excitons can play a role in the photoelectric emission from these materials. This opens an opportunity for experimental examination of exciton transport and dynamics.

ACKNOWLEDGMENTS

The authors gratefully acknowledge the loan of the McPherson VUV monochromator by W. E. Spicer. The natural diamond single crystal was kindly provided by Dr. F. A. Raal of the DeBeers Diamond Laboratory, Johannesburg. This work was supported by NSF under Grant No. ECS-9222368. C.B. acknowledges the WSU graduate school and the E.E. Donaldson Scholarship fund for partial support.

[1]A. Einstein, Ann. Phys. **17**, 132 (1905).
[2]*Photoemission and the Electronic Properties of Surfaces,* edited by B. Feuerbacher, B. Fitton, and R. F. Wills (Wiley, New York, 1978).
[3]C. S. Fadley, in *Synchrotron Radiation Research: Advances in Surface and Interface Science,* edited by R. S. Bachrach (Plenum, New York, 1992), Vol. 1, p. 421.
[4]W. E. Spicer, Phys. Rev. **112**, 114 (1958).
[5]W. E. Spicer, Appl. Phys. **12**, 115 (1977).
[6]C. Bandis and B. B. Pate, Phys. Rev. Lett. **74**, 777 (1995).
[7]R. L. Bell, *Negative Electron Affinity Devices* (Clarendon, Oxford, 1973).
[8]W. E. Pickett, Phys. Rev. Lett. **73**, 1664 (1994).
[9]J. van der Weide *et al.*, Phys. Rev. B **50**, 5803 (1994).
[10]I. Lindau and W. E. Spicer, J. Electron. Spectrosc. Relat. Phenom. **3**, 409 (1974).
[11]F. J. Himpsel *et al.*, Phys. Rev. B **20**, 624 (1979).
[12]B. B. Pate *et al.*, J. Vac. Sci. Techol. **19**, 349 (1981).
[13]B. B. Pate, Surf. Sci. **165**, 83 (1986).
[14]F. J. Himpsel *et al.*, Phys. Rev. B **24**, 7270 (1981).
[15]J. van der Weide and R. J. Nemanich, Appl. Phys. Lett. **62**, 1878 (1993).
[16]J. van der Weide and R. J. Nemanich, J. Vac. Sci. Technol. B **10**, 1940 (1992).
[17]C. Bandis, D. Haggerty, and B. B. Pate, in *Diamond, SiC and Nitride Wide Bandgap Semiconductors,* edited by C. H. Carter, Jr., G. Gildenblat, S. Nakamura, and R. J. Nemanich, MRS Symposia Proceedings No. 339 (Materials Research Society, Pittsburgh, 1994), p. 75.
[18]J. van der Weide and R. J. Nemanich, J. Vac. Sci. Technol. B **12**, 2475 (1994).
[19]D. P. Malta *et al.*, in *Diamond, SiC and Nitride Wide Bandgap Semiconductors* (Ref. 17), p. 39.
[20]D. P. Malta *et al.* (unpublished).
[21]J. van der Weide and R. J. Nemanich, Phys. Rev. B **49**, 13 629 (1994).
[22]P. J. Dean, E. C. Lightowlers, and D. R. Wight, Phys. Rev. **140**, A352 (1965).
[23]F. Wooten, *Optical Properties of Solids* (Academic, New York, 1972).
[24]T. P. McLean, *Progress in Semiconductors* (Wiley, New York, 1960), Vol. 5, p. 55.
[25]R. J. Elliott, Phys. Rev. **108**, 1384 (1957).
[26]R. S. Knox, in *Solid State Physics: Advances in Research and Applications,* edited by F. Seitz and D. Turnbull (Academic, New York, 1963), Vol. 5.
[27]J. Singh, *Solid State Physics: Advances in Research and Applications* (Academic, New York, 1984), Vol. 38, p. 295.
[28]G. Davies, in *Properties of Diamond,* edited by J. E. Field (Academic, London, 1979), p. 165.
[29]C. D. Clark, P. J. Dean, and P. V. Harris, Proc. R. Soc. London Ser. A **277**, 312 (1964).
[30]G. Dresselhaus, J. Phys. Chem. Solids **1**, 14 (1956).
[31]M. Altatelli and N. O. Lipari, Phys. Rev. B **15**, 4898 (1977).
[32]N. O. Lipari and M. Altarelli, Phys. Rev. B **15**, 4883 (1977).
[33]J. Kono *et al.*, Phys. Rev. B **48**, 10 917 (1993).
[34]F. Nava *et al.*, Solid State Commun. **33**, 475 (1980).
[35]W. E. Spicer, in *Optical Properties of Solids—New Developments,* edited by B. O. Seraphin (North-Holland, Amsterdam, 1976), p. 631.
[36]The diamond single crystal, *D*5, was provided on loan by Dr. F. A. Raal from DeBeers Diamond Laboratory, Johannesburg.
[37]H. Emanuel, *Diamonds and Precious Stones* (Putnam's, New York, 1873).
[38]J. Wilks and E. Wilks, *Properties and Applications of Diamond* (Butterworth, Heinmann, 1991), Chap. 9.
[39]M. J. Dresser, M. D. Alvey, and J. T. Yates, Surf. Sci. **169**, 91 (1986).
[40]C. Bandis, Ph.D. thesis, Washington State University, 1994.
[41]K. Y. Yu, Ph.D. thesis, Stanford University, 1976.
[42]N. J. Shevchik, Rev. Sci. Instrum. **47**, 1028 (1976).
[43]J. N. Miller, Ph.D. thesis, Stanford University, 1979.
[44]J. Samson, *Techniques of Vacuum Ultraviolet Spectroscopy* (Wiley, New York, 1967), p. 214.
[45]K. Watanabe and E. C. Y. Inn, J. Opt. Soc. Am. **43**, 32 (1953).
[46]W. F. Krolikowski and W. E. Spicer, Phys. Rev. B **1**, 478 (1970).
[47]B. J. Waclawski *et al.*, J. Vac. Sci. Technol. **21**, 368 (1982).
[48]B. B. Pate *et al.*, J. Vac. Sci. Technol. **21**, 364 (1982).
[49]A. V. Hamza, G. D. Kubiak, and R. H. Stulen, Surf. Sci. Lett. **206**, L833 (1988).
[50]K. C. Pandey, Phys. Rev. B **25**, 4338 (1982).
[51]D. J. Chadi, J. Vac. Sci. Technol. A **2**, 948 (1984).
[52]D. Vanderbilt and S. G. Louie, Phys. Rev. B **30**, 6118 (1984).
[53]B. B. Pate *et al.*, J. Vac. Sci. Technol. A **2**, 957 (1984).
[54]J. F. Morar *et al.*, Phys. Rev. B **33**, 1340 (1986).
[55]B. B. Pate *et al.*, in *Science and Technology of New Diamonds,* edited by S. Saito (KTK, Tokyo, 1990), p. 345.
[56]G. D. Kubiak and K. W. Kolasinski, Phys. Rev. B **39**, 1381 (1989).
[57]J. F. Morar *et al.*, Phys. Rev. B **33**, 1340 (1986).
[58]A. V. Hamza, G. D. Kubiak, and R. H. Stulen, Surf. Sci. **237**, 35 (1990).
[59]G. S. Painter, D. E. Ellis, and A. R. Lubinsky, Phys. Rev. B **4**, 3610 (1971).
[60]B. D. Thoms *et al.*, J. Chem. Phys. **100**, 8425 (1994).
[61]The curve fit in the inset of Fig. 6 was performed using an asymmetric Lorentzian function convoluted with a Gaussian. The centroid of the surface-state emission was found to be at −2.4 eV.
[62]J. van der Weide, Ph.D. thesis, North Carolina State University, 1993.
[63]E. C. Lightowlers and A. T. Collins, J. Phys. D **9**, 951 (1976).
[64]A. T. Collins and A. W. S. Williams, J. Phys. C **4**, 1789 (1971).
[65]J. E. Field, *Properties of Diamond* (Academic, London, 1979), p. 131.
[66]S. M. Sze, *Physics of Semiconductor Devices,* 2nd ed. (Wiley, New York, 1981).
[67]Y. P. Varshini, Physica **34**, 149 (1967).
[68]J. Wilks and E. Wilks, *Properties and Applications of Diamond* (Ref. 38), p. 81.
[69]J. D. Jackson, *Classical Electrodynamics,* 2nd ed. (Wiley, New York, 1975), p. 287.
[70]R. A. Roberts and W. C. Walker, Phys. Rev. **161**, 730 (1967).
[71]B. B. Pate, I. Lindau, and W. E. Spicer, *Proceedings of the 17th International Conference on the Physics of Semiconductors,* edited by J. D. Chadi and W. A. Harrison (Springer-Verlag, Berlin, 1985), p. 1183.
[72]R. Gomer, *Field Emission and Field Ionization* (Harvard University Press, Cambridge, MA, 1961).
[73]M. H. Hecht, J. Vac. Sci. Technol. B **8**, 1018 (1990).
[74]C. Bandis and B. B. Pate (unpublished).
[75]B. B. Pate, Ph. D. thesis, Stanford University, 1984.
[76]M. D. Sturge, in *Excitons,* edited by E. I. Rashba and M. D. Sturge, Modern Problems in Condensed Matter Sciences (North Holland, Amsterdam, 1982), p. 20.
[77]C. Klingshirn, in *Optical Properties of Excited States,* edited by

B. Di Bartolo (Plenum, New York, 1992), p. 119.
[78]J. P. Wolfe, Phys. Today **35** (3), 46 (1982).
[79]H. Y. Fan, Radiat. Eff. **4**, 7 (1970).
[80]J. L. Warren *et al.*, Phys. Rev. **158**, 805 (1967).
[81]J. Kalcher and A. F. Sax, Chem. Phys. Lett. **150**, 99 (1988).
[82]M. Rei Vilar *et al.*, Europhys. Lett. **5**, 375 (1988).
[83]R. L. Bell, *Negative Electron Affinity Devices* (Clarendon, Oxford, 1973), Appendix C, p. 127.
[84]G. W. Gobeli, F. G. Allen, and E. O. Kane, Phys. Rev. Lett. **12**, 94 (1964).
[85]E. O. Kane, Phys. Rev. Lett. **12**, 97 (1964).
[86]D. E. Alburger, in *Encyclopedia of Physics,* edited by R. G. Lerner and G. L. Trigg (VCH, New York, 1991), p. 93.
[87]M. C. Benjamin *et al.*, Appl. Phys. Lett. **64**, 3288 (1994).
[88]M. C. Benjamin *et al.*, in *Diamond, SiC and Nitride Wide Bandgap Semiconductors* (Ref. 17), p. 39.
[89]N. Schwentner, E.-E. Koch, and J. Jortner, in *Electronic Excitations in Condensed Rare Gases,* edited by G. Höhler, Springer Tracts in Modern Physics Vol. 107 (Springer-Verlag, Berlin, 1985).
[90]D. A. Lapiano-Smith *et al.*, Appl. Phys. Lett. **59**, 2174 (1991).
[91]E. M. Gullikson and A. P. Mills, Jr., Phys. Rev. B **39**, 6121 (1989).

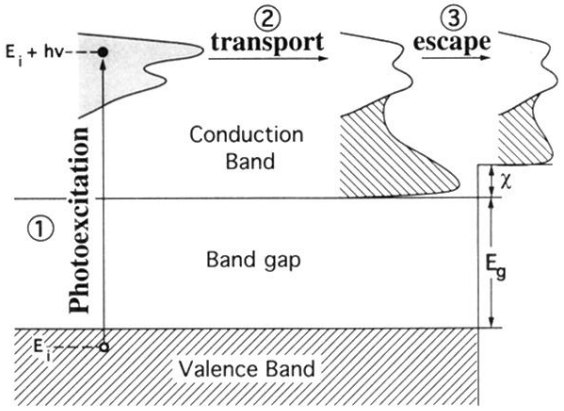

FIG. 2. The three-step model of photoemission. (1) photoexcitation, (2) transport, (3) escape (after Ref. 35).